Electronic supporting information

For

# Exploring the homopolar dehydrocoupling of ammonia borane by solid-state multinuclear NMR spectroscopy

Binayak Roy*†, Urbi Pal‡, Ankita Bishnoi*, Luke O'Dell‡, Pratibha Sharma*

*Department of Energy Science and Engineering, Indian Institute of Technology Bombay, India

†School of Chemistry, Monash University, Clayton, Australia

‡Institute for Frontier Materials, Deakin University, Geelong Waurn Ponds, Australia

## Experimental procedure

**Preparation of the post dehydrogenated product**

Ammonia borane (AB, 90% purity) and aluminium phosphate (AP) was procured from Sigma-Aldrich Australia, and used without any further purification. 100 mg of ammonia borane was dissolved in 5 ml of THF at room temperature. The solution then was slowly added to 100 mg of aluminium phosphate and stirred at 200 rpm for 3 hours. The dispersion was placed under vacuum in a Schlenk line for the removal of THF solvent. The vacuum evaporation resulted in the elimination of THF solvent, and the resulting powder had AB impregnated within the porous structure of AP. This powder was named as AB+AP and stored in glove box at room temperature. The post heated decomposed samples have been prepared by heating the ammonia borane samples under dynamic heating condition. The AB and AB+AP samples were heated in a STF-16 tubular furnace from room temperature to 300°C under the heating rate of 10°C/min in Ar atmosphere. The post heated products of pure and supported AB were further analysed through solid state 2D NMR spectroscopy.

**NMR data acquisition and analysis details**

All solid-state NMR experiments were carried out at $B_0$ = 11.75 T using a 500 MHz Bruker Avance III NMR spectrometer, equipped with a 1.3 mm ultra-fast MAS probe and a 62.5 kHz MAS rate. The samples were packed in MAS zirconia rotors in a glovebox under an argon atmosphere to minimize contact with moisture. The chemical shifts of $^{11}$B and $^{1}$H are reported in ppm referenced to boron trifluoride diethyl etherate ($Et_2O$-$BF_3$) and nitromethane, respectively. $^{14}$N overtone frequencies are reported in kHz due to the MAS-rate dependent position of the overtone signals, as detailed elsewhere in the literature[1], and were referenced using the overtone signal from glycine.

The $^{1}$H-$^{14}N^{OT}$ HMQC spectra were acquired with a standard HMQC pulse sequence but with WURST-80 pulses on the $^{14}N^{OT}$ channel in order to improve the excitation bandwidth (200 µs duration, 100 kHz sweep range). 256 scans were acquired for each slice with a 2 s recycle delay, and 128 slices were acquired in the indirect dimension with a $t_1$ increment of 8 µs.

The $^{11}$B MQMAS spectrum was obtained using a 3 pulse split-$t_1$ pulse sequence, 60 scans acquired for each slice with a 1 s recycle delay, and 196 slices acquired in the indirect dimension with a $t_1$ increment of 16 µs.

The $^{1}$H-$^{11}$B HETCOR spectra were obtained with a 2.5 ms contact time, a ramped contact pulse on the $^{1}$H channel, 32 scans acquired for each slice with a 2 s recycle delay, and 128 slices acquired in the indirect dimension with a $t_1$ increment of 50 µs.

All spectra were processed using the Bruker TopSpin software, with the "xfshear" command applied in the case of the MQMAS spectrum.

Table S1: The $^{11}B$ MQMAS model fitting parameters of the product of supported AB

| | $\delta_{obs}$ | $\delta_{iso}$ | $C_Q$ (kHz) | $\eta_Q$ | $P_Q$ (kHz) | Assignment |
|---|---|---|---|---|---|---|
| Site 1 | 32.66 | 28.34 | 2784 | 0.17 | 2797 | Peripheral $BN_2H$ |
| Site 2 | 30.65 | 26.66 | 2716 | 0.27 | 2749 | Internal $BN_3$ |
| Site 3 | 27.42 | 24.01 | 2718 | 0.28 | 2754 | Peripheral $BN_3$ |
| Site 4 | 23.44 | 19.9 | 2588 | 0.24 | 2612 | **Homopolar Boron site** |
| Site 5 | 1.64 | 1.25 | - | - | | $BN_4$ |

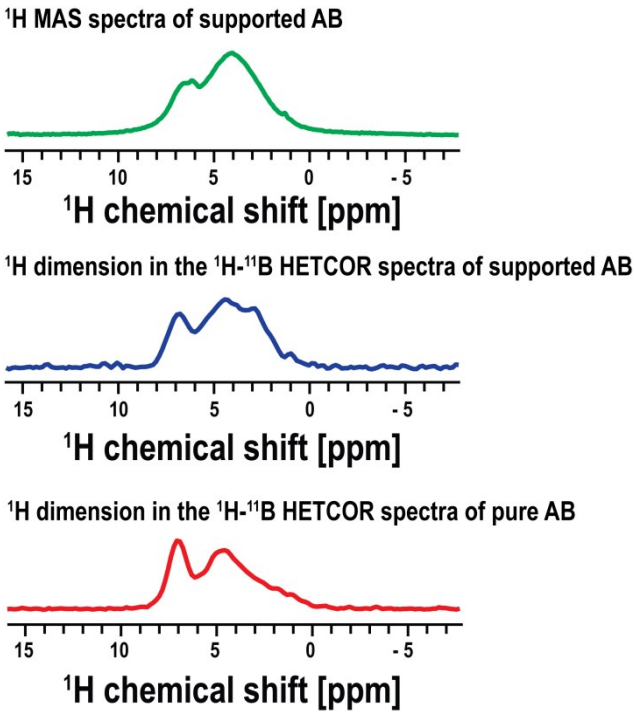


Figure S1: The $^1H$ chemical shifts of supported AB and pure AB as observed in $^1H$ MAS and 2D $^1H$-$^{11}B$ HETCOR analysis

A comparison (Figure S1) between the $^1H$ MAS and 2D $^1H$-$^{11}B$ HETCOR spectra of the supported AB shows that the HETCOR analysis reveals much more detailed information than its $^1H$ MAS spectra. A comparison between the HETCOR spectra of supported and pure AB shows a significantly different $^1H$ chemical shift profile, which may arise from the involvement of B-B interaction.

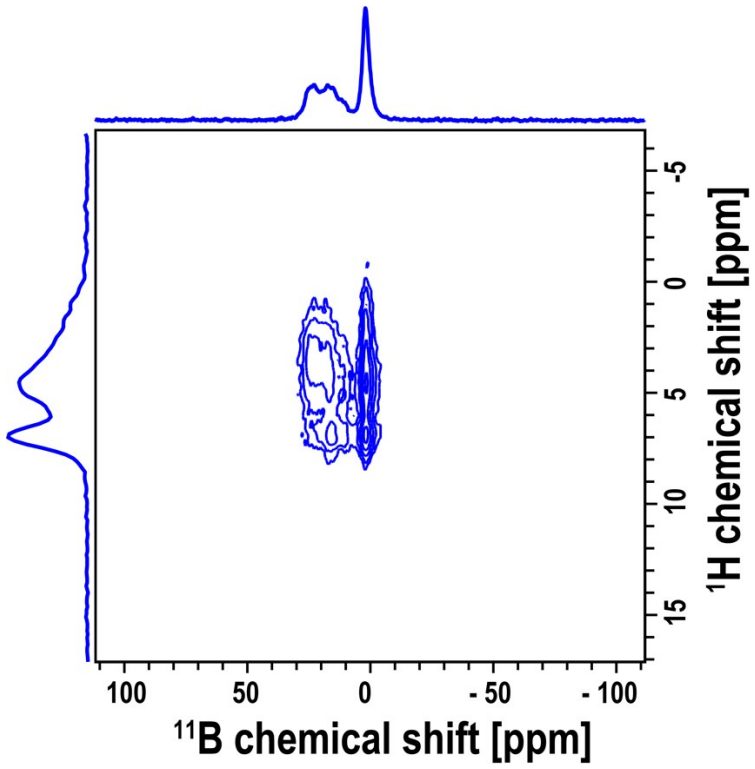


Figure S2: Solid state $^{1}$H-$^{11}$B HETCOR NMR spectra of the post dehydrogenated product of pure AB depicting the $^{1}$H and $^{11}$B chemical shifts along the Y and X axis, respectively

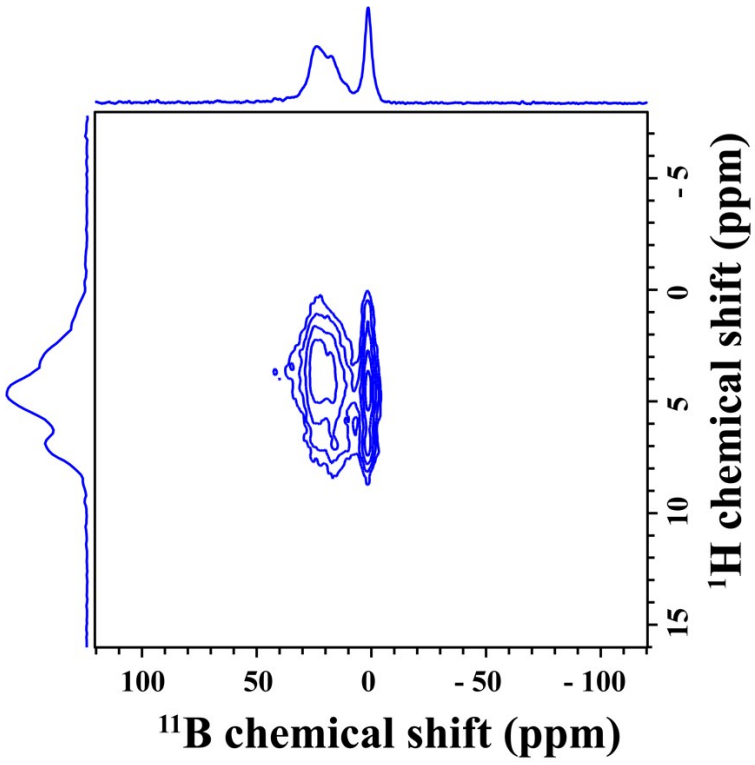


Figure S3: Solid state $^{1}$H-$^{11}$B HETCOR NMR spectra of the post dehydrogenated product of supported AB depicting the $^{1}$H and $^{11}$B chemical shifts along the Y and X axis, respectively for the contact time of 2 ms

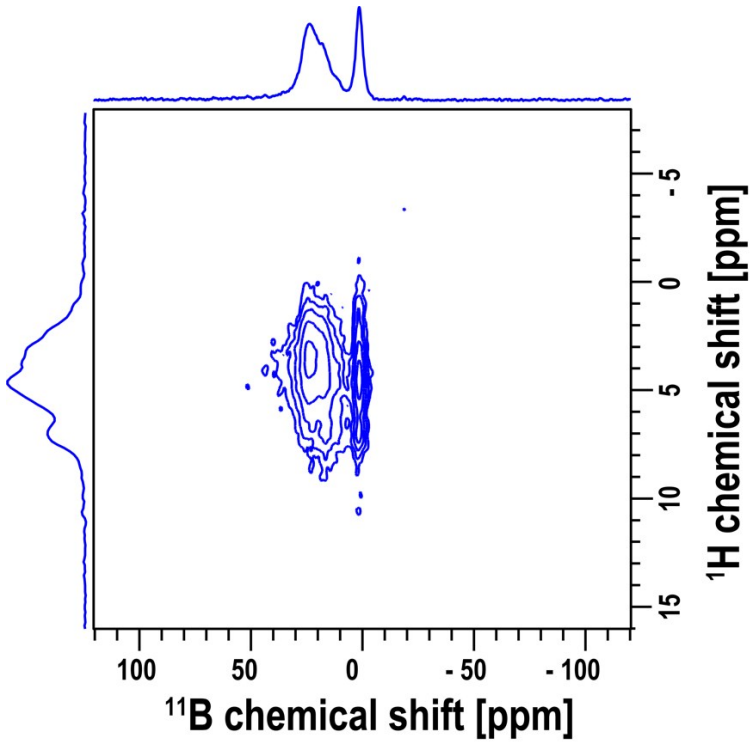


Figure S4: Solid state $^{1}$H-$^{11}$B HETCOR NMR spectra of the post dehydrogenated product of supported AB depicting the $^{1}$H and $^{11}$B chemical shifts along the Y and X axis, respectively for the contact time of 1 ms

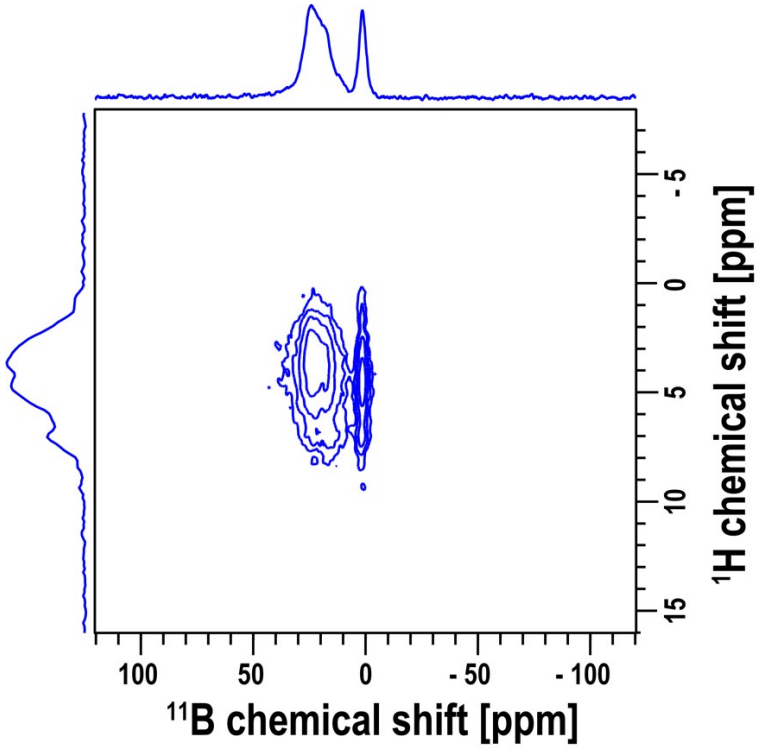


Figure S5: Solid state $^{1}$H-$^{11}$B HETCOR NMR spectra of the post dehydrogenated product of supported AB depicting the $^{1}$H and $^{11}$B chemical shifts along the Y and X axis, respectively for the contact time of 0.5 ms

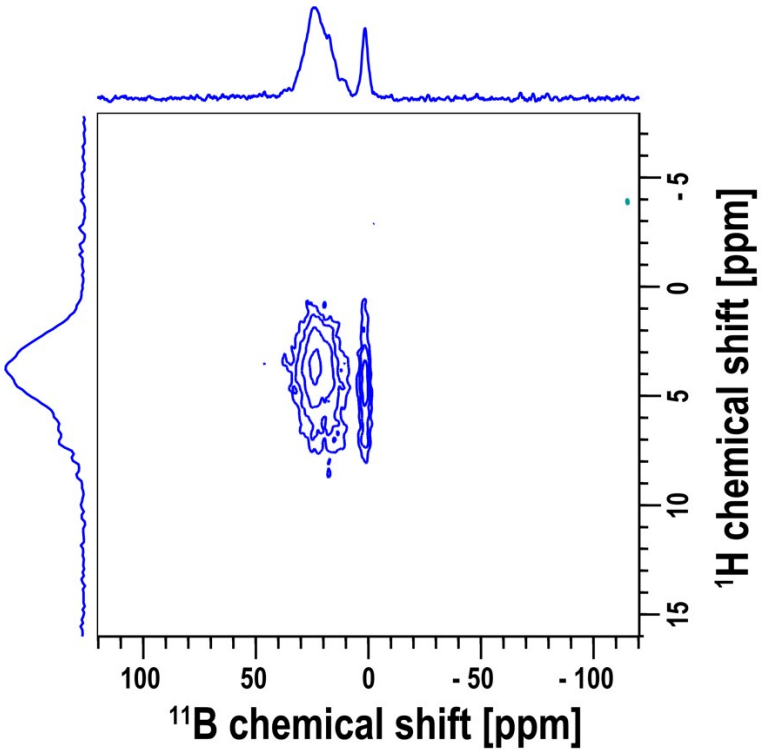


Figure S6: Solid state $^{1}$H-$^{11}$B HETCOR NMR spectra of the post dehydrogenated product of supported AB depicting the $^{1}$H and $^{11}$B chemical shifts along the Y and X axis, respectively for the contact time of 0.25 ms

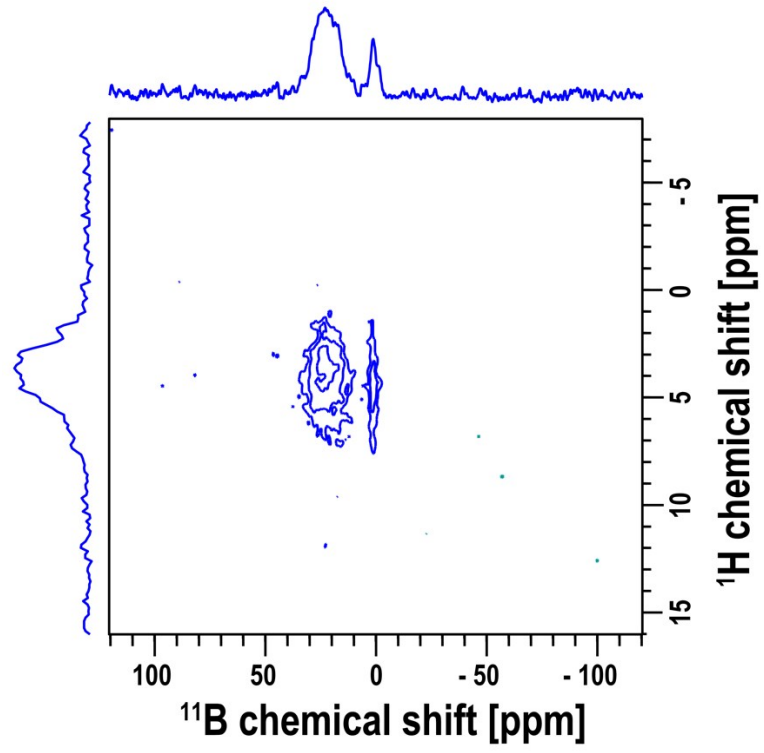


Figure S7: Solid state $^{1}$H-$^{11}$B HETCOR NMR spectra of the post dehydrogenated product of supported AB depicting the $^{1}$H and $^{11}$B chemical shifts along the Y and X axis, respectively for the contact time of 0.1 ms

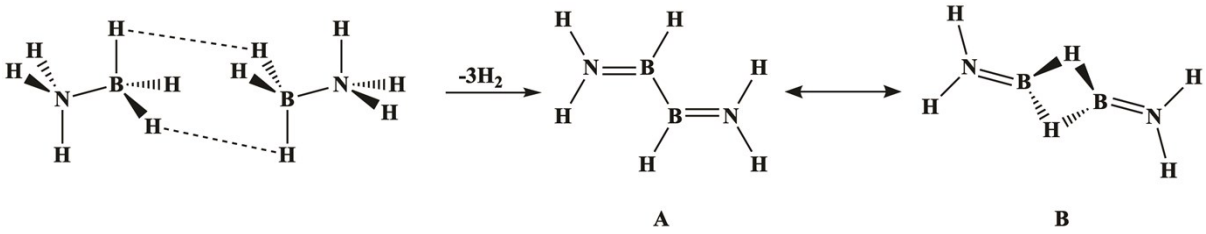


Figure S8: A schematic representation of homopolar B-B interaction in the ammonia borane decomposition

The $^{1}H$ spectra at each individual contact time has been fitted assuming the presence of only $^{1}H$ species at 4.5, 3.5 and 2.7 ppm, as seen in the HETCOR spectra. However, additional peaks may also be present which are masked by the anisotropic broadening of the solid sample.

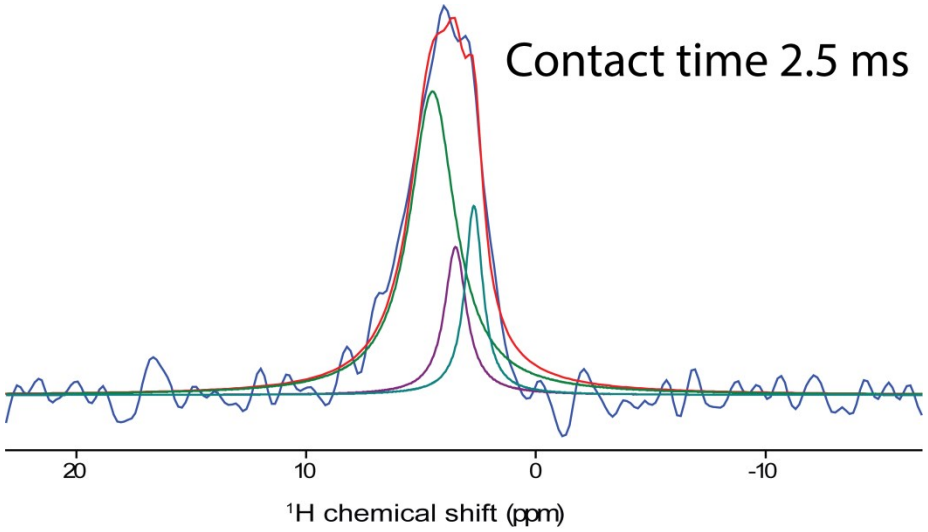


Figure S9: $^{1}H$ peak fit of the $^{1}H$ spectra coupled with the planar B(III) site at the contact time of 2.5 ms

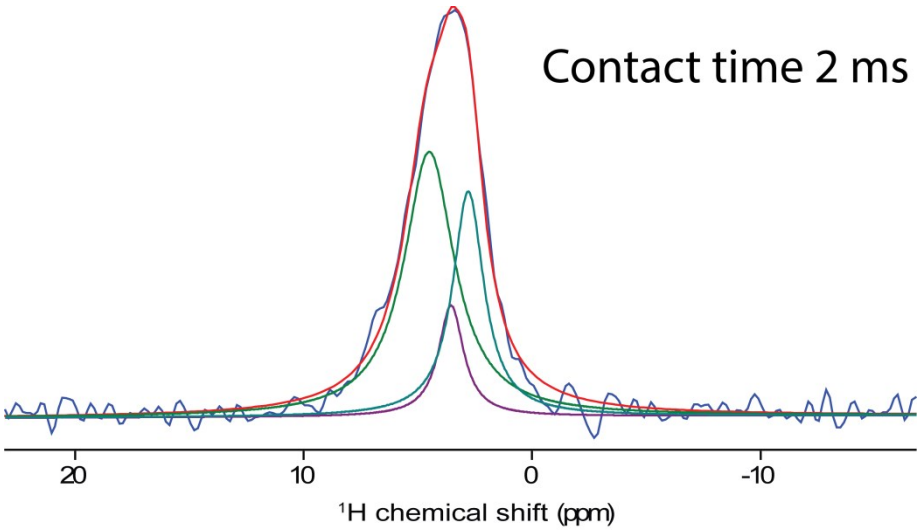


Figure S10: $^{1}H$ peak fit of the $^{1}H$ spectra coupled with the planar B(III) site at the contact time of 2 ms

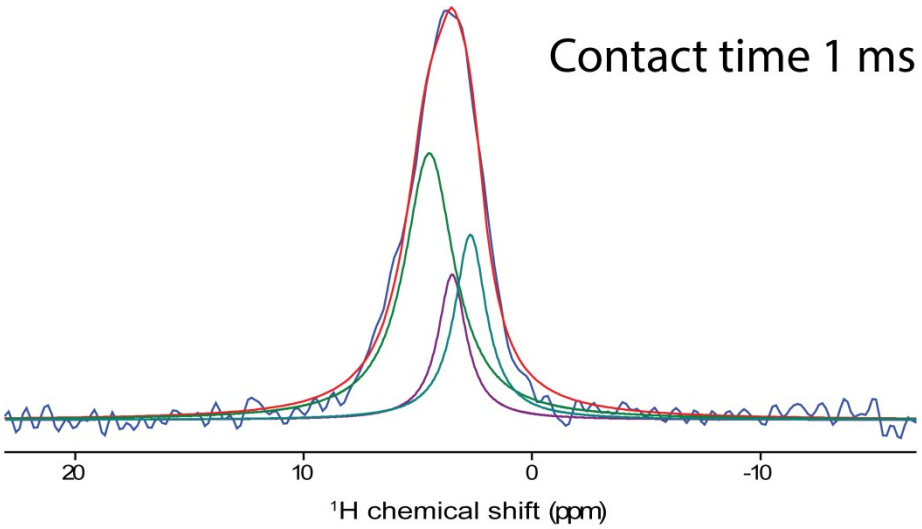


Figure S11: $^{1}H$ peak fit of the $^{1}H$ spectra coupled with the planar B(III) site at the contact time of 1 ms

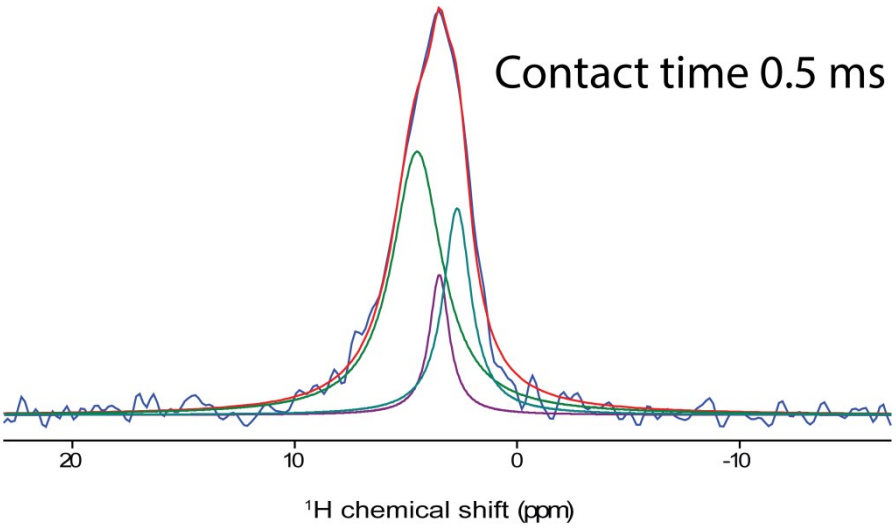


Figure S11: $^{1}H$ peak fit of the $^{1}H$ spectra coupled with the planar B(III) site at the contact time of 0.5 ms

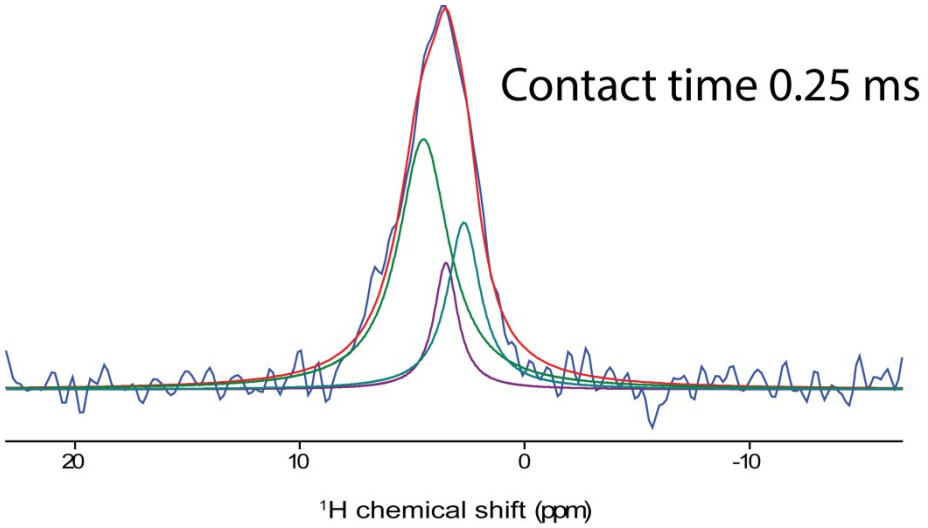


Figure S13: $^{1}H$ peak fit of the $^{1}H$ spectra coupled with the planar B(III) site at the contact time of 0.25 ms.

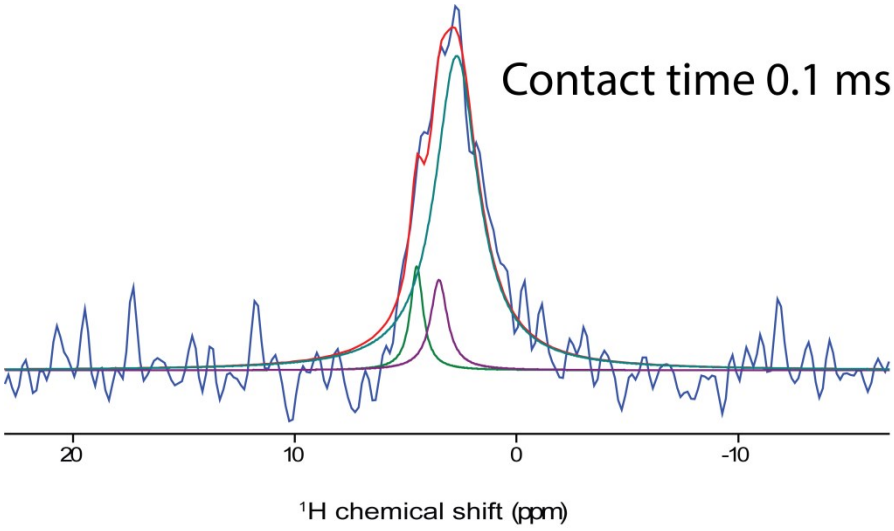


Figure S14: $^{1}$H peak fit of the $^{1}$H spectra coupled with the planar B(III) site at the contact time of 0.1 ms.

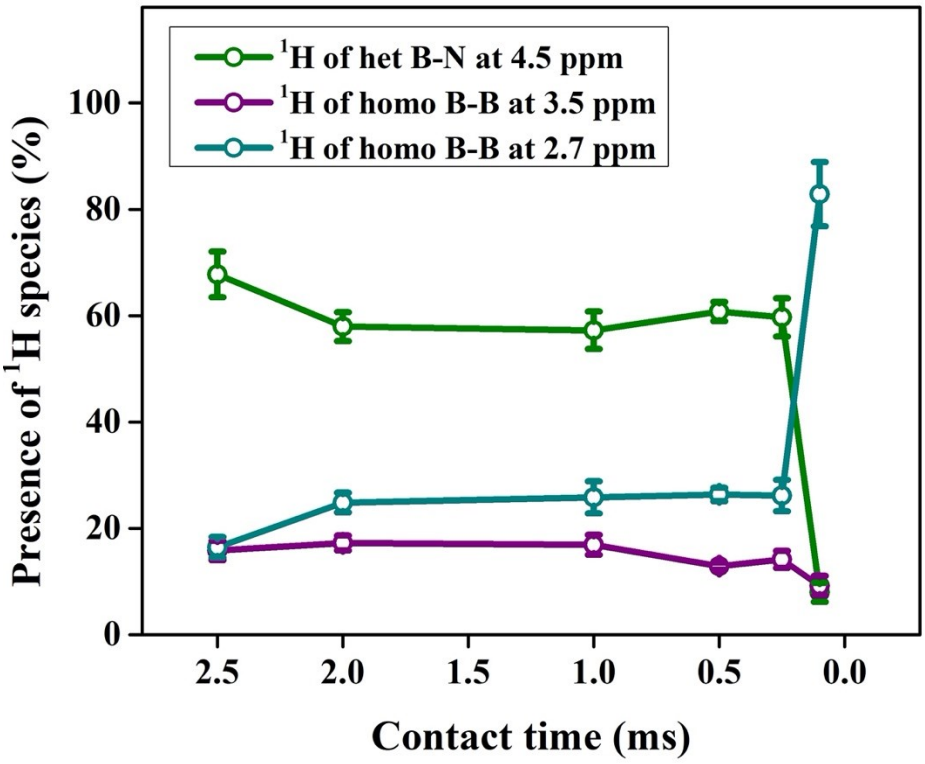


Figure S15: percentile presence of $^{1}$H sites coupling with $^{11}$B (III) sites as a function of contact time.